doi:10.1038/nature09392

1 Deterministic loading of the spin ground state and measurement of the Zeeman energy splitting

We have employed a modified pulsing sequence (Fig. S1a) to demonstrate the ability to deterministically load the spin-down state, and read it out accordingly. We started from a three-level pulse as shown in Fig. 1b of the main article, and fixed the Read level at its optimal value for correct spin readout. We then set up a sequence where the Load level is scanned over a large range. To avoid artefacts that may arise due to a varying step height before the Read phase, we added a Plunge phase between Load and Read, set at a level identical to the fixed Load level used in Fig. 2. The result is shown in Fig. S1b. For high Load levels, no electron is loaded because the donor electrochemical potentials during the Load phase are higher than that of the SET, for both spin states. An electron with random spin is then loaded during the Plunge phase, and yields the characteristic peak of $\langle I_{\rm SET}\rangle$ at the beginning of the Read pulse, due to the current pulses caused by $|\uparrow\rangle$ electrons. When the load level becomes comparable with the Read level, then $\mu_\downarrow < \mu_{\rm SET} < \mu_\uparrow$ and only $|\downarrow\rangle$ electrons can be loaded. The subsequent Plunge pulse has no effect, since a $|\downarrow\rangle$ electron has already occupied the donor. Accordingly, we measure no spin-up signals during the Read phase. Further lowering the Load level yields $\mu_\downarrow, \mu_\uparrow < \mu_{\rm SET}$ and allows the loading of both spin states, as revealed by the reappearance of spin-up signals in the Read phase.

This experiment is relevant from a quantum information perspective. It shows that it is possible to initialize the spin to its ground state by means of electrical pulses, on a time scale determined by the electron tunnel time ~ 10 μs. This means it is not necessary to wait a time $\sim T_1$ – which can exceed one second, as shown in Fig. 3d – to have a well-defined initial spin state.

The voltage range $\Delta V_\downarrow$ where only spin-down electrons are loaded corresponds to the energy interval where $\mu_\downarrow < \mu_{\rm SET} < \mu_\uparrow$. Therefore, this experiment yields the Zeeman energy splitting of the electron spin, $E_{\rm Z} = g\mu_{\rm B}B$, after converting the voltages into energies through the expression $E_{\rm Z} = \alpha e \Delta V_\downarrow$, where α is the lever arm of the gates, and $e = -1.6 \times 10^{-19}$ C is the elementary charge. To find the lever arm we apply a compensated triangular wave to the top and plunger gates, and measure the average current through the SET at $B = 0$. Here, $\langle I_{\rm SET}\rangle$ goes from high to low or vice versa when crossing the charge transition point (Fig. S2a). The width of the transition is proportional to the width of the Fermi distribution of electron states in the SET island. Thus we fit $\langle I_{\rm SET}\rangle$ to the function

$$\langle I_{\rm SET}(V_{\rm pulse})\rangle = \frac{a}{1+\exp\left[\frac{eV_{\rm pulse}-b}{c}\right]} + d \qquad (1)$$

where a, b, c and d are fitting parameters. The fitting parameter c has units of energy; dividing c by the Boltzmann constant yields a parameter $c/k_{\rm B}$, with units of temperature but including the lever arm α. Repeating the experiment at different bath temperatures and plotting the

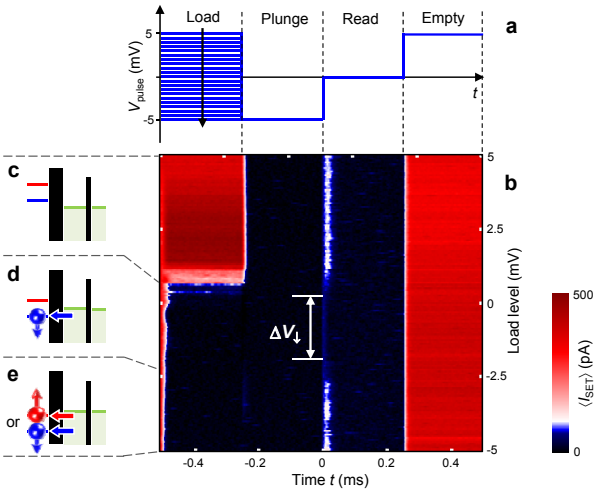

Figure 1: **Deterministic loading of the spin-down state. a** Four-level pulsing sequence. The Load level is scanned from +5 to -5 mV. A Plunge phase at $V_{\rm pulse} = -5$ mV is introduced to ensure that the step before the Read phase remains constant. **b** $\langle I_{\rm SET} \rangle$ as a function of time and of the $V_{\rm pulse}$ level during the load phase, with 256 averages, $B = 4$ T and 30 kHz bandwidth. **c** High Load level: The high $\langle I_{\rm SET} \rangle$ signals that no electron is loaded during the Load phase, but is loaded during the Plunge, in either the $|\downarrow\rangle$ or $|\uparrow\rangle$ state. Some $|\uparrow\rangle$ states are detected during the Read phase. **d** Load level comparable to read: Only $|\downarrow\rangle$ states are loaded. No $|\uparrow\rangle$ states detected, confirming the validity of the readout method. **e** Low Load level: Both states can be loaded, and detected accordingly.

extracted $c/k_{\rm B}$ against $T_{\rm bath}$ yields the data in Fig. S2b. At $T_{\rm bath} > 250$ mK, $c/k_{\rm B}$ is linear in temperature and can be written as $c/k_{\rm B} = T_{\rm bath}/\alpha$. Therefore, the lever arm $\alpha \approx 0.28$ is found by taking the inverse of the slope of the best fit through these points (the red line in Fig. S2b). At $T < 250$ mK, $c/k_{\rm B}$ deviates from the linear behaviour, indicating that the electron temperature in the SET island deviates from $T_{\rm bath}$, and saturates to a value $T_{\rm el} \approx 200$ mK. Multiplying by α the values of $\Delta V_\downarrow$ obtained at different magnetic fields, we find $E_{\rm Z}(B)$ as shown in Fig. S2c. The field dependence of the measured $E_{\rm Z}$ is in good agreement with the calculated value for electron spins in Si with gyromagnetic ratio $g = 2$.

2 Measurement and analysis of the spin relaxation rate $T_1^{-1}(B)$

2.1 Single-shot *vs.* averaged spin relaxation measurements

Having demonstrated the ability to read out the electron spin state in single-shot, the spin relaxation rate T_1^{-1} can be obtained by measuring the fraction of spin-up counts $P_\uparrow$ as a function of the wait time $\tau_{\rm w}$ before the spin is read, as shown in Fig. 3. However we note that measuring T_1 does not strictly require single-shot readout. Since the spin-up current pulses occur with the highest probability in a well defined time interval, the average current $I_{\rm SET}(t)$ has a Poissonian shape (Fig. S3b), and its integral is proportional to $P_\uparrow$. Figure S3c shows that the integral of $I_{\rm SET}(t)$ for $0 < t < 100$ μs can be rescaled and superimposed with $P_\uparrow$ as obtained from single-shot readout, and an exponential fit of the form $P_\uparrow(\tau_{\rm w}) = P_\uparrow(0)\exp(-\tau_{\rm w}/T_1)$ yields the same T_1 for both methods.

The method of integrating the averaged current flowing through a quantum point contact has been recently used to measure the spin lifetime in Si/SiGe (Ref. 25) and Si/SiO_2 (Ref. 26) quantum dots, where the signal-to-noise ratio was not sufficient to achieve single-shot readout.

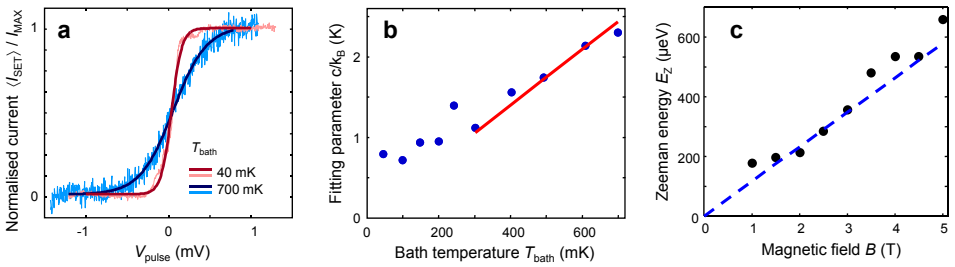

Figure 2: **Lever arm calibration and extraction of the electron spin g-factor. a** $\langle I_{\rm SET}\rangle$ resulting from a triangular wave swept between -1.25 and $+1.25$ mV, as a function of the $V_{\rm pulse}$ level at fridge temperatures of 40 and 700 mK. **b** Fitting parameter, $c/k_{\rm B}$, versus bath temperature, $T_{\rm bath}$. The inverse of the slope of the red line through the points at $T > 250$ mK yields a lever arm $\alpha \approx 0.28$. **c** Zeeman splitting $E_{\rm Z}$ of the electron spin versus magnetic fields B. $E_{\rm Z}$ is extracted from the four level pulse experiment of Fig. S1 and converted in energy units using the α value obtained in panel **b**. The data are in good agreement with the values calculated for $g = 2$ electron spins in silicon (dashed line).

Counting spin excited states in single-shot provides an absolute measure of $P_\uparrow$, but is otherwise equivalent to the averaged current method for T_1 measurements.

2.2 High-T vs. low-T limits of the spin-lattice relaxation mechanism

The spin-lattice relaxation rates for P donors in Si, in the temperature regime $T < 2$ K where only one-phonon processes are relevant, have been calculated by Hasegawa[24] and Roth[31]. Both calculations deal with a spin-lattice relaxation mechanism where the spin-orbit coupling is modulated by crystal strain. Because the strain breaks the equivalence of the 6 conduction band minima of silicon ("valleys"), it affects the anisotropy of the electron g-factor. The two models describe two different – both valid – ways in which the breaking of valley degeneracy influences the g-factor anisotropy, and give qualitatively similar results but different angular dependencies. The Hasegawa's "valley repopulation" model predicts no relaxation when $B \parallel [100]$, while the "single valley" model of Roth yields a finite contribution for all field orientations. The magnetic field in our experiment is oriented along the [110] direction, thus both mechanisms give a contribution. A comprehensive discussion and experimental test of both relaxation mechanisms has been given by Wilson and Feher[32].

Both the above models have been written in the high-temperature limit, $k_{\rm B}T \gg g\mu_{\rm B}B$. The formula of Hasegawa[24], for example, reads:

$$T_1^{-1}(B) = f_{\rm Si}(\theta,\phi)\frac{6}{5\pi}\left(\frac{g'\Xi}{3g\Delta E}\right)^2\left(\frac{1}{\rho\nu_t^5}+\frac{2}{3\rho\nu_l^5}\right)\left(\frac{g\mu_{\rm B}B}{\hbar}\right)^4 k_{\rm B}T, \tag{2}$$

$$= K_4 B^4 T \tag{3}$$

where $f_{\rm Si}(\theta,\phi)$ is an angular factor of order unity, $g = 1.9985$ is the gyromagnetic ratio of the electron bound to a P donor, $\Xi \approx -7$ eV is a parameter that describes the energy shift of the conduction band minima ("valleys") due to a deformation of the crystal lattice, $g' = (g_l - g_t)/3$ describes the anisotropy of the g-factor along the principal axes of the effective mass tensor for each valley, ΔE is the energy difference between the first excited valley state and the ground state, $\rho = 2330$ kg/m^3 is the density of Si, and $\nu_t = 5860$ m/s and $\nu_l = 8480$ m/s are the transverse and longitudinal sound velocities, respectively.

All the material– and donor–dependent properties can be condensed in a parameter K_4 which is explicitly independent of B and T in the regime of interest. A $B-$dependence of K_4 would

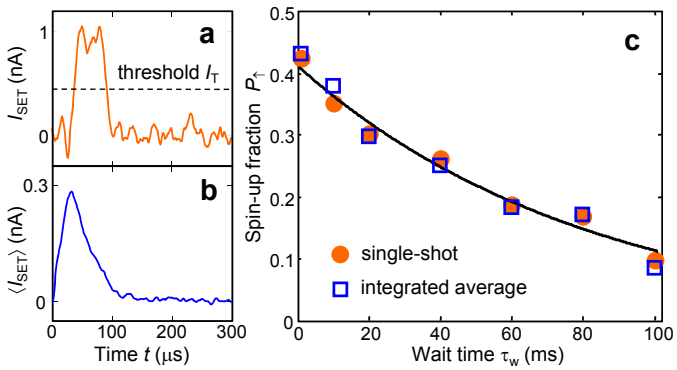

Figure 3: **Single-shot vs. averaged spin lifetime (T_1) measurements. a** Example of single-shot trace. A state $|\uparrow\rangle$ is counted when $I_{\rm SET} > I_{\rm T} = 0.45$ nA (dashed line). **b** Average of 500 single-shot traces. **c** The spin-up fraction $P_\uparrow(\tau_{\rm w})$ can be obtained by counting the $|\uparrow\rangle$ states in single-shot (dots) or by integrating $\langle I_{\rm SET}\rangle$ (squares). Rescaling and normalizing $\langle I_{\rm SET}\rangle(\tau_{\rm w})$ shows that the two approaches are equivalent and can be fitted by the same exponential decay (solid line). Data taken on Device A at $B = 5$ T.

arise if the wavelength of the emitted phonon became comparable with the Bohr radius of the donor wavefunction. However, this would require $B \gg 50$ T for Si:P and is therefore not relevant here. The remaining $\propto B^4T$ dependence contains a contribution $(1+N_{\rm ph}) \approx k_{\rm B}T/g\mu_{\rm B}B$, where $N_{\rm ph} = 1/[\exp(g\mu_{\rm B}B/k_{\rm B}T) - 1]$ is the Bose factor for the thermal occupation of the phonon modes with energy $g\mu_{\rm B}B$. This factor is included to describe both spontaneous and stimulated emission of a phonon upon relaxation of the excited spin state.

The low-T limit of Eq. (2), $k_{\rm B}T \ll g\mu_{\rm B}B$, can be obtained by replacing $(1+N_{\rm ph})$ with 1, i.e. considering only spontaneous phonon emission in the derivation of $T_1^{-1}(B)$ (see e.g. Ref. 23), which becomes:

$$T_1^{-1}(B)|_{{\rm low}-T} = K_4 \frac{g\mu_{\rm B}B}{k_{\rm B}T} B^4 T = K_5 B^5. \tag{4}$$

This is the $\propto B^5$ contribution to the relaxation rate we have found in our experiment (Fig. 3d). For the coefficients K_4 and K_5 the following relationship holds:

$$K_4 = \frac{k_{\rm B}}{g\mu_{\rm B}} K_5. \tag{5}$$

Feher and Gere[7] measured the T_1^{-1} of P donors in a natural-isotope, bulk-doped ($n \sim 10^{16}$ cm^{-3}) Si crystal at $B = 0.32$ T parallel to the [100] direction, down to $T = 1.25$ K, obtaining $T_1^{-1} \approx 2 \times 10^{-4}$ s^{-1}, corresponding to a spin lifetime $T_1 \sim 1.4$ hours and a coefficient $K_4 \approx 0.015$ s^{-1}T^{-4}. Using Eqs. (3) and (5), we can extrapolate the results of Feher and Gere to the low-T regime, obtaining $K_5 \approx 0.02$ s^{-1}T^{-5}. This is higher by a factor ≈ 1.3 as compared to the single-spin results we obtained on Device B, and a factor ≈ 2.6 compared to Device A. As noted by Feher and Gere[7], when measuring such long relaxation times the presence of trace amounts of paramagnetic impurities can play an important role, and lead to the observation of artificially high relaxation rates.

The data point shown in Fig. 3d (J.J.L. Morton, private communication), measured on a bulk Si:P crystal at $B = 3.35$ T and $T < 5$ K, can be compared directly to the single-spin results, because it is measured already in the low-T regime, $k_{\rm B}T < g\mu_{\rm B}B$. The bulk spin relaxation rate is in this case a factor ≈ 1.3 below the line $T_1^{-1}(B) = K_{5{\rm A}}B^5$ of Device A, and a factor ≈ 2.6 below the line $T_1^{-1}(B) = K_{5{\rm B}}B^5$ of Device B.

Equation (2) indicates that $T_1^{-1} \propto \Delta E^{-2}$, i.e. the spin lifetime is reduced when the valley-orbit splitting decreases. It has been shown that donors in gated nanostructures[33] can have ΔE values much lower than in bulk. Therefore the slight difference between our data and the bulk Si:P result, and the variability between the two devices we have measured, can be accounted for by a variation of ΔE due to electric fields and proximity to the Si/SiO_2 interface.

2.3 B-independent contribution – spin diffusion

The spin relaxation rate $T_1^{-1}(B)$ shown in Fig. 3d for Device A contains a field-independent contribution, $K_{0A} = 1.84 \pm 0.07$ s^{-1}. We suggest that this contribution arises from spin diffusion, due to the dipolar coupling of the measured spin to the electron spins on neighboring P donors. The device contains an expected 18 donors (Poisson statistics) in a 90×90 nm^2 area, corresponding to an average inter-donor distance $d \approx 24$ nm. The dipolar coupling Hamiltonian contains a "flip-flop" term, which allows two spins to swap their orientation. Although this mechanism conserves the total energy of the spin system, when a spin-up electron loaded on the single donor under measurement undergoes a flip-flop with a neighbouring spin, it will appear to have relaxed to the spin-down state if measured after some time.

In a natural-isotope silicon crystal, each donor site is subject to an inhomogeneous broadening of the local magnetic field due to the hyperfine coupling with ^{29}Si nuclei[6], with half-width $\langle \Delta\omega_I \rangle = g\mu_B \langle B_I \rangle / \hbar$, where $\langle B_I \rangle \approx 0.125$ mT. $\langle B_I \rangle$ is much larger than the mutual dipolar field between electron spins at distances > 10 nm, and has the effect of suppressing the energy-conserving flip-flops. An order of magnitude of the flip-flop rate Γ_{ff} of two electron spins S at distance d can be obtained from a Fermi golden rule argument[34]:

$$\Gamma_{ff} \approx \frac{\pi}{2\langle \Delta\omega_I \rangle} M_{ff}^2(\theta, d), \tag{6}$$

where $\hbar M_{ff}$ is the strength of the flip-flop matrix element in the dipolar Hamiltonian, dependent on the distance d and the angle θ that the vector joining the donors makes with the external field. The term $\pi / \langle \Delta\omega_I \rangle$ in Eq. (6) plays the role of a density of states, and the additional factor 2 in the denominator accounts for the effect of ^{31}P nuclei, which can have equal or opposite direction in the two donors. Using $d = 24$ nm and averaging over θ we obtain $\Gamma_{ff} \approx 2$ s^{-1}, comparable with the experimental result. A more accurate estimate of Γ_{ff} would require summing the contributions of all neighbouring donors, a detailed knowledge of their location, and whether they are neutral or ionized.

3 Readout fidelity and calculation of the distribution of peak currents $N_\uparrow(I_p)$, $N_\downarrow(I_p)$

We have modelled the measurement fidelity with a numerical algorithm that accurately reproduces the experimental setup. The model, illustrated in Fig. S4, proceeds along the following steps:

i. Randomly assign a spin state, $|\downarrow\rangle$ or $|\uparrow\rangle$ with a probability $P_\downarrow$ or $P_\uparrow$, respectively. For $|\downarrow\rangle$ states, a trace with $I_{SET} = 0$ is created. For $|\uparrow\rangle$ states, a spin-up signal is generated, which includes a current pulse of height $\Delta I = 1.9$ nA, as observed in the experiment. To simulate spin-up signals with the correct statistical properties, we generate for each trace two random numbers, r_{out} and r_{in}, with uniform probability distributions between 0 and 1. We thus define a pulse that starts after a delay $\tau_{\uparrow,out} = -\log(r_{out})/\Gamma_{\uparrow,out}$ and lasts a time $\tau_{\downarrow,in} = -\log(r_{in})/\Gamma_{\downarrow,in}$, with $\Gamma_{\uparrow,out} = 10$ μs and $\Gamma_{\downarrow,in} = 40$ μs as obtained from the

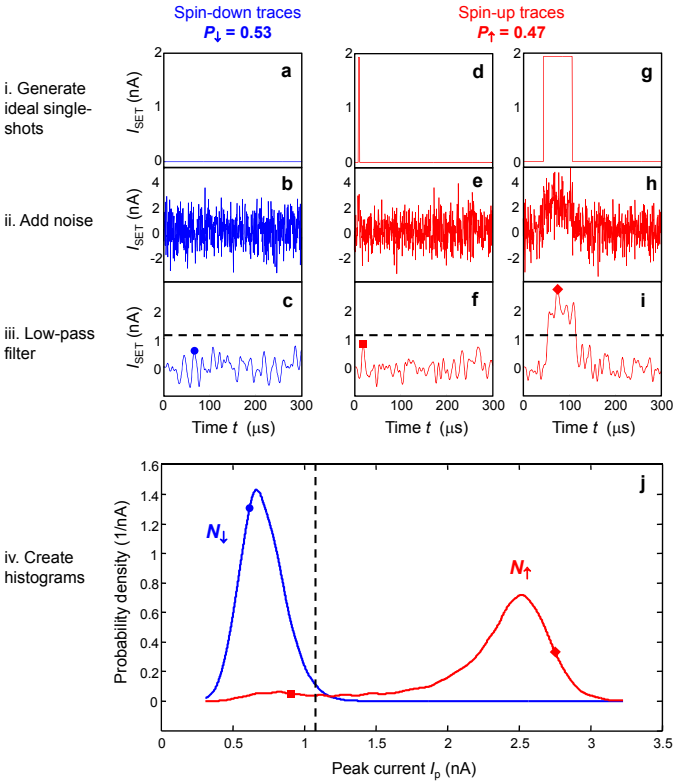

Figure 4: **Calculation of the peak current distributions.** Examples of the steps involved in calculating $N_\downarrow(I_\mathrm{p})$ and $N_\uparrow(I_\mathrm{p})$, as explained in the text. **a** – **c** Spin-down traces. **d** – **i** Spin-up traces. **j** Calculated histograms, with the parameters that yield the best fit to the data in Fig. 4b. In **c, f** and **i** the circle, square and diamond are the detected peak current values for each trace, and are reported in panel **j** accordingly. The dashed lines represent the optimal threshold current $I_\mathrm{T} = 1.1$ nA.

fits to the experimentally observed tunnel times in Fig. 4d,e.

ii. Add random Gaussian noise with amplitude A_n to each trace.

iii. Apply a numerical filter with the same 8^{th} order, 120 kHz low-pass Bessel function as used in the experimental setup.

iv. For each simulated trace, find the peak value I_p of $I_\mathrm{SET}(t)$ in the interval $0 < t < 100$ μs. This value is used to construct the histograms $N_\downarrow(I_\mathrm{p})$ and $N_\uparrow(I_\mathrm{p})$, which represent the probability that a spin-down or spin-up electron produces a single-shot trace with a peak current value I_p. Here we can obtain separately $N_\downarrow(I_\mathrm{p})$ and $N_\uparrow(I_\mathrm{p})$ because we know a priori which spin state corresponds to each trace.

The only free parameters in the model are the noise amplitude A_n and the spin-up fraction $P_\uparrow$. We start with an initial choice of A_n and $P_\uparrow$, generate $N_\downarrow(I_\mathrm{p})$ and $N_\uparrow(I_\mathrm{p})$ from 80,000 simulated traces, then run an optimization algorithm to find the best agreement between the

simulated histograms and the experimental result, as shown in Fig. 4b. An example of the simulation is shown in Fig. S4. In particular, we show two different examples of spin-up signals, one of which is a current pulse of very short duration (Fig. S4d). Due to the low-pass filtering, such a short current pulse results in a low peak current (Fig. S4f). In a single-shot readout experiment, a trace like this would be erroneously interpreted as spin-down.

Supplementary references

31. Roth, L. *Massachusetts Institute of Technology Lincoln Laboratory Reports*, April 1960 (unpublished).

32. Wilson, D. K. & Feher, G. Electron spin resonance experiments on donors is silicon. III. Investigation of excited states by the application of uniaxial stress and their importance in relaxation processes. *Phys. Rev.* **124,** 1068–1083 (1961).

33. Lansbergen, G. P. *et al.* Gate-induced quantum-confinement transition of a single dopant atom in a silicon FinFET. *Nat. Phys* **4,** 656 (2008).

34. Mims, W. B. in *Electron Paramagnetic Resonance*, edited by S. Geschwind (Plenum Press, New York, 1972).